A SILICON MICROMACHINED, FEEDBACK CONTROLLED 2D MICROPOSITIONER WITH SUB-NANOMETER RESOLUTION

Larry L. Chu[1,2] and Yogesh B. Gianchandani[1,2]
[1]Department of Electrical and Computer Engineering, University of Wisconsin, Madison, WI 53706
[2]EECS Department, University of Michigan, Ann Arbor, MI 48109

ABSTRACT

This paper reports on a multi-purpose two-axis micropositioner with sub-nanometer position sensing for precise feedback control. Along each axis it has an electrothermal actuator, a capacitive position sensor, and a displacement amplifier that provides a gain of 3.37 for the sensor. It is fabricated from custom SOI wafers using dry etching, and each component is electrically and thermally isolated by silicon nitride. For a fabricated device of 65 µm thickness, the measured displacement sensitivity is 0.333 fF/nm, which corresponds to 0.3 nm resolution with available laboratory instrumentation. The range is ≈19 µm for the positioner, which corresponds to 66 µm travel in the sense combs. Using a parallel inductor, a positioning displacement of 9.6 µm offers a shift of 240 KHz in L-C resonance, supporting sub-nm resolution.

I. INTRODUCTION

Micromachined devices are typically batch manufactured using fabrication technologies that matured in the integrated circuits industry. By integrating mechanical structures and electrical circuitries in hybrid or monolithic microsystems, complex electro-mechanical functionalities become feasible. The resulting products often benefit from being cheaper, smaller, and more reliable than conventionally machined counterparts.

Micropositioners have been constructed in the past using various actuators such as electrostatic [1], magnetic [2,3], and thermal actuators [4,5], amongst others. Positioners are needed for many applications such as scanning microscopy, optical switching, wireless communications, and data storage. Due to variations in manufacturing and operating conditions, high precision positioners must be operated with feedback control. While some system applications provide this capability with secondary means of position sensing [1], most do not. Ultimately, the resolution of a feedback controlled positioner is limited by its ability to sense location in a precise manner over a wide dynamic range. While a 100 nm resolution positioner with built-in position sensing was reported in [2], this was an electromagnetic metal device with one axis of motion. This paper describes a batch fabricated Si device with two axes (2D) of motion and sub-nanometer resolution.

The multi-purpose micropositioner design described in this work operates in-plane, meaning that the motions are parallel to the substrate. The 1D positioner design is composed of bent-beam electrothermal actuators [4], compliant displacement amplifiers [6], capacitive sensor banks, sample stage area, and interconnect. These components are shown in a schematic drawing in Fig. 1; the actuator is connected to the sample stage and the amplifier simultaneously. The displacement of the sample stage is amplified by the compliant structure and sensed by the capacitive banks. Since they are used exclusively for sensing, they can be densely packed without fear of electromechanical instability. The compliant mechanism does not undergo mechanical loading at the capacitive sensor end because no net electrostatic force is exerted during sensing. The signals at the sample stage can be transferred off-chip using the interconnect spring and pad. The sample stage is electrically isolated from the actuator, which is isolated from the amplifier and sensors. The two dimensional micropositioner has two symmetrical actuation mechanisms arranged orthogonally. The two mechanisms are connected to the tip area with a long shank. The isolation plugs shown in Fig. 1 electrically separate the sample stage, the actuator, and the position sensor.

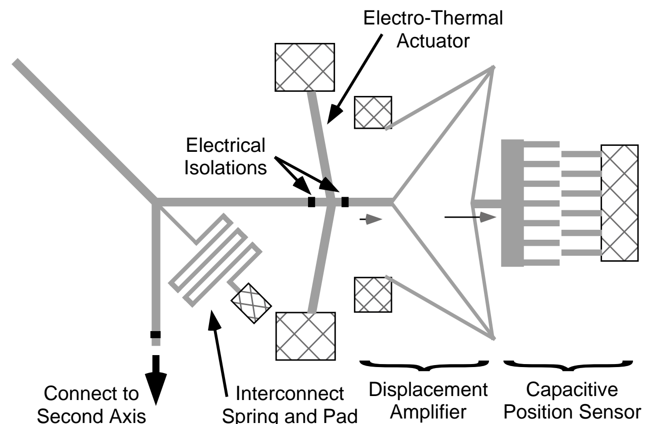

Fig. 1: Schematic drawing of a 2D positioner showing the actuator, the amplifier, and the capacitive sensor.

The electrothermal bent-beam actuator is an excellent transducer of strain to displacement [7]. Joule heating in the bent-beam results in mechanical strain due to thermal expansion, which is translated into mechanical displacement by the bent-beam structure. The actuator is designed to provide sufficient force and displacement to drive the rest of

the elements in the system. Its behavior can be described using three parameters: D_{max}, the maximum unloaded displacement (Fig. 2a), F_{max}, the maximum loading force that nullify the unloaded displacement (Fig. 2b), and the mechanical spring constant of the actuator, K_{eq}, which is typically the ratio between these. It can be expressed as [4]:

$$K_{eq} = \frac{2 \cdot \sin^2(\theta_1) \cdot A \cdot E}{L_1} \quad (1)$$

where A is the crossection area, L_1 is the length of the bent-beam, θ_1 is the bending angle, and E is the Young's modulus of the material.

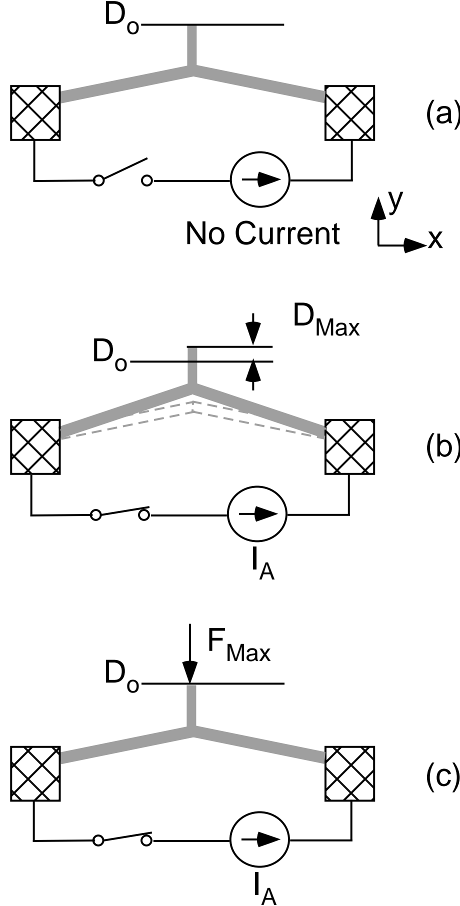

Fig. 2: The actuation characteristics of a bent-beam actuator can be characterized with D_{max}, the maximum unloaded displacement, and F_{max}, the maximum loading force.

II. FABRICATION

The micropositioner is fabricated from silicon-on-insulator (SOI) substrates made with fusion wafer bonding. Two wafers, one device wafer and one handle wafer, are cleaned and thermally oxidized to form 1.7 µm SiO_2. The handle wafer is 540 µm thick and the device wafer has an initial thickness of 650 µm. The resistivity of the handle wafer is not crucial, but the device layer is highly conductive single crystal silicon (0.001 to 0.005 Ohm-cm). The low resistivity device layer is necessary in order to provide suitable V-I behavior for the electrothermal actuators. The two oxidized substrates are brought into contact for wafer bonding, followed by a slow temperature ramp to 950 ˚C for fusion bonding. The bonded substrate is kept at high temperature for 1 hour before a slow ramp down.

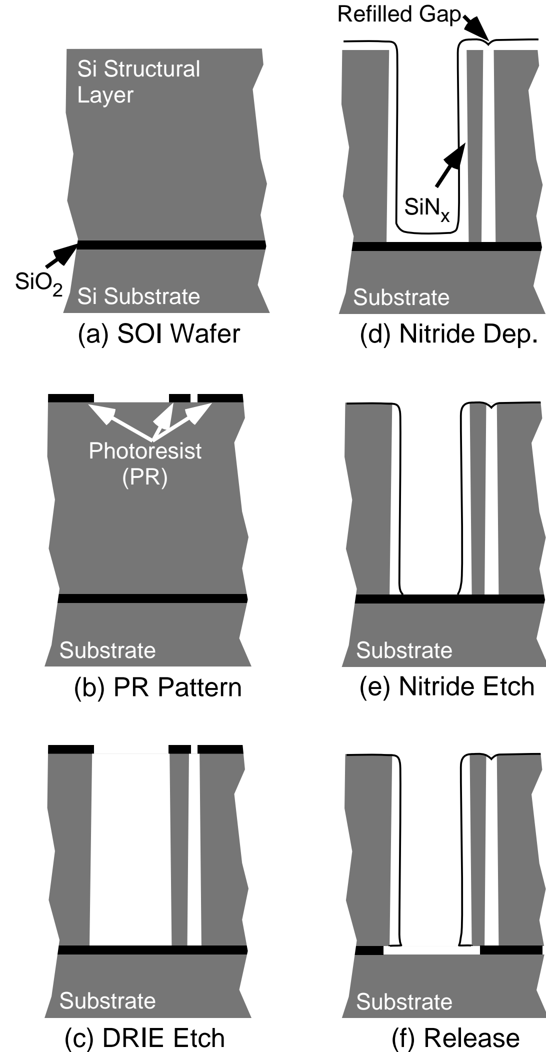

Fig. 3: Fabrication of micropositioner using SOI substrates.

The device layer of the bonded SOI stack is thinned to the desired thickness by first grinding and polishing the device side to a thickness of 100 µm. Then, a SF_6-based plasma in a parallel plate reactor is used to thin the stack to the final desired thickness. It was found that the surface of the device layer was acceptable for photolithography even after 4 hours of dry etching (up to 50 µm of removal).

The SOI wafer is then patterned using a deep reactive ion etching (DRIE) step with 3.5 µm of photoresist as masking material (Fig. 3c). Deep reactive ion etching uses the Bosch process [8], a Fluorine based chemistry that allows high-aspect ratio etches using alternating etch and side-wall

passivation steps. Inductively coupled plasma (ICP) is used in this etch step to provide high plasma density while keeping the mean ion energy low, which allows the use of photoresist as a etch mask. After the etch terminates on the buried oxide layer, the wafer is cleaned and a 2.3 µm layer of low-stress LPCVD nitride is deposited to form the electrical isolations using a trench refill process (Fig. 3d); this step does not require extra masks to achieve electrical isolations. The excessive nitride is removed using a blanket etch (Fig. 3e), leaving only nitride on the sidewall of the structure and in the refilled plugs. This etch step was done in two stages: first, 80% of the thickness is removed with a SF_6-based plasma, then, a CHF_3 plasma is used for the removal of the reminder of the nitride. CHF_3 is used because it has a selectivity of about 10:1 for nitride and silicon (the selectivity of nitride and oxide is also excellent). Finally, the device is released in 6:1 buffered oxide etchant (BOE) for 45 minutes and dried using a supercritical CO_2 process (Fig 3f). Figure 4 shows the optical picture of the 2D positioner; the inserts shows the sidewall profile of the structure. In the left insert, the elbow of the displacement amplifier is shown; the sidewall nitride layer can be seen as the layer which appears brighter than the silicon exposed at the top of the structure. Electrical isolation plugs are the result of the nitride refilling steps described earlier. A SEM of the plugs is shown in Fig. 4.

III. MEASUREMENT RESULTS

The 1D operation of the structure is verified by applying power to one of the actuators and monitoring the sensor capacitance (HP 4284A) in the actuation direction. At the same time, the capacitive position measurements are verified by optical displacement measurements taken with an imaging system. The results are shown in Fig. 5; tip displacement is the displacement measured at the input of the amplifier. The tine displacement is essentially the displacement seen by the capacitive sensor. A 15.1 µm tip displacement requires ≈14 V and 100 mA, and generates a tine displacement of 50.3 µm and a capacitance change of 2.93 pF. The amplification factor of the compliant displacement amplifier is measured to be 3.37 from this measurement. This compares well with the FEA predictions (Fig. 6). Also, the sensitivity of the capacitive sensor is found to be 0.333 fF/nm in the intended region of operation, and the behavior is well predicted with numerical models (Fig. 7). The numerical simulation considers 10 tine pairs. With an electrical setup that can reliably measure 0.1 fF, which is routinely achievable using standard laboratory instruments, this sensitivity corresponds to a displacement accuracy of 0.3 nm. If on-chip electronics are used, the displacement sensitivity can be further improved.

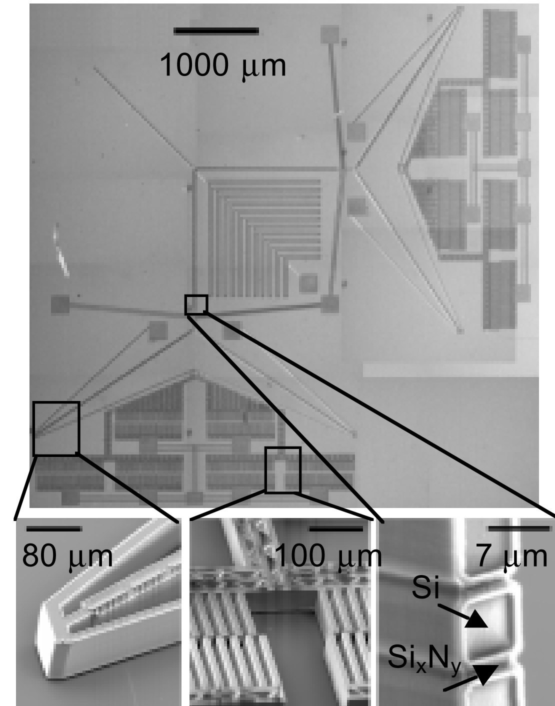

Fig. 4: Optical image of positioner (above) and close-up SEM images of: the elbow microtransmission (left); capacitive tines (center), and Si_xN_y plugs (right).

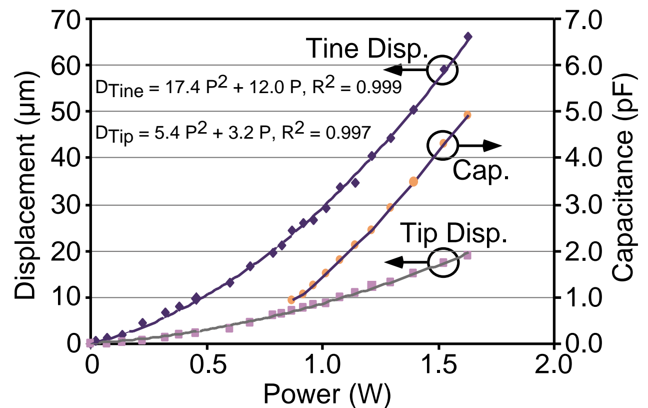

Fig. 5: By applying power to one of the actuators, the capacitance of the sensor is measured simultaneously with the displacements.

In any 2D positioner with orthogonally placed flexural drives, when one side is actuated, a small displacement is geometrically imposed on the other one (Fig. 8). Although it is easy to null this by actuating the passive axis by a small amount, it is instructive to measure the uncompensated cross-talk. In this device the cross-talk (measured capacitively) corresponded to 105 nm for actuated displacement of 14.6 µm, which is ≈-43 dB of isolation. The fact that the cross axial error is picked up by the capacitive sensor illustrates well that the structure can be operated to compensate for this effect.

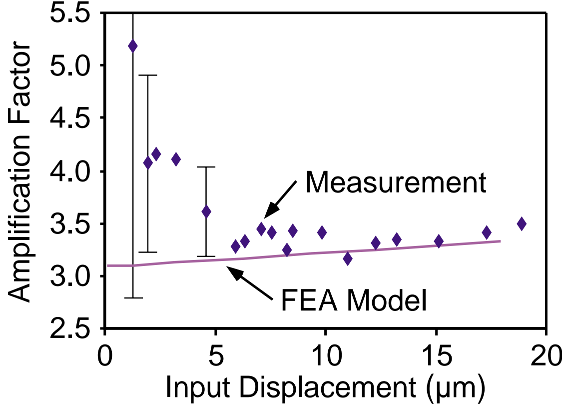

Fig. 6: Measurement and modeling of mechanical amplification factor.

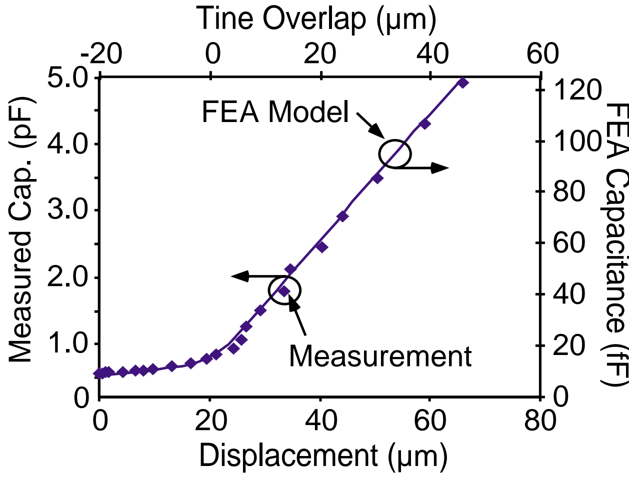

Fig. 7: Measurement and modeling of the capacitance sensor bank response. The sidewall nitride refilling effect is used as a fitting factor.

The 2D operation of the device is demonstrated by actuating the two actuators simultaneously and measuring the capacitance change of both sensor banks. This result is shown in Fig. 9. The shading in these two plots indicates the capacitance levels. Straight bands of shading would be considered ideal. Figure 9a shows the capacitance of the X-axis sensor, while Fig. 9b shows the response of the Y-axis sensor. The non-idealities are primarily due to the cross-axial behavior just described.

Finally, the capacitance change in the sensor bank can be used in a simpler pickup technique, namely resonance shift method. By connecting a 100 µH inductor in parallel to the capacitive sensor, one can measure the resonance behavior of the structure. As the sense capacitance changes, the resonance peak shifts. This method is demonstrated in Fig. 10, where it is clear that the resonance peak shifted 240 KHz over 9.6 µm of tip displacement. This is a relatively large shift, and testifies to the high resolution capability of this device.

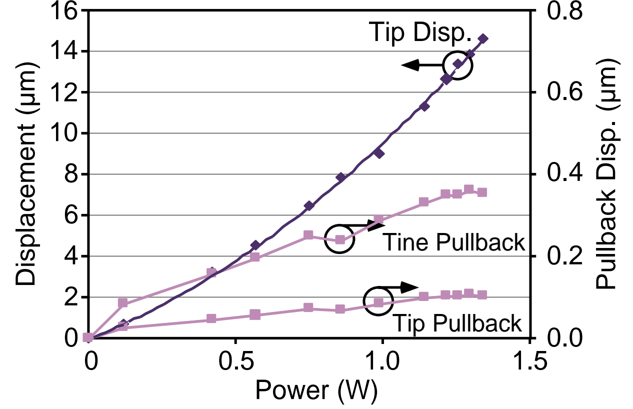

Fig. 8: Power is applied to one axis, and the displacement error caused by this actuation at the other axis is measured and plotted.

The shifting of the resonance frequency is consistent with the electrical behavior of the circuit model shown in Fig. 11, where C is the sensor response, L is the external inductor, R_L is the series resistance in the inductor, C_P is the parasitic capacitance, and R is the leakage resistance. The lowering of the resonance quality factor, Q, is attributed to series resistances in the measurement setup and the external inductive element.

IV. THERMAL-MECHANICAL NOISE

Thermal-mechanical noise (TMN) is a factor that can potentially limit the positioning resolution of the device. It arises from molecular agitation in and around the mechanical structure such as Brownian motion. The theoretical treatment of calculating TMN is detailed in [9] for a mass-spring-damper mechanical system. The thermal-mechanical noise force density, F, can be found using:

$$F = \sqrt{4 \cdot k_B \cdot T \cdot D} \tag{2}$$

where k_B is the Boltzman's constant, T is the absolute temperature, and D is the damping of the system; F has a unit of [N/√Hz]. In order to obtain the damping, D, the resonance frequency of the system is obtained using finite-element analysis (FEA). The damping can be found using:

$$D = \frac{\sqrt{K \cdot M}}{Q_M} \tag{3}$$

where K is the stiffness of the structure, M is the mass, and Q_M is the mechanical quality factor. Finally, the displacement due to TMN can be found using the following equation:

$$X_{TM-Noise} = \frac{F \cdot \sqrt{f_{res1}}}{K} = \frac{\sqrt{4 \cdot k_B \cdot T \cdot D \cdot f_{res1}}}{K} \tag{4}$$

where f_{res1} is the frequency of the fundamental mode resonance. Assuming a Q_M of 1~10 (which is typical for such a system), the displacement due to TMN is calculated to be less than 1.1 pico meter. This result indicates that TMN will not be a significant source of displacement error.

V. CONCLUSION

A feedback controllable 2D positioner was designed, fabricated, and tested. The unique construction allows the structure to achieve 19 μm displacement at sub-nanometer resolution (~0.3 nm). The capacitance change can be measured with standard laboratory instruments to provide sub-nanometer displacement accuracy. Also, using a parallel LC resonant circuit, a frequency shift of 240 KHz is obtained over 9.6 μm tip displacement, corresponding to a resolution of 25 Hz/nm. Both methods are suitable for high resolution displacement measurements. The estimated positioning error due to thermal-mechanical noise is less than 1.1 pico meter, which is well below the target resolution.

ACKNOWLEDGEMENTS

The authors are grateful to Dr. Joel Hetrick for the initial design of the displacement amplifier [6], and Dr. Mo-huang Li for the assistance with the temperature distribution measurement of the thermal actuators. This effort was supported in part by an NSF Career award to YG.

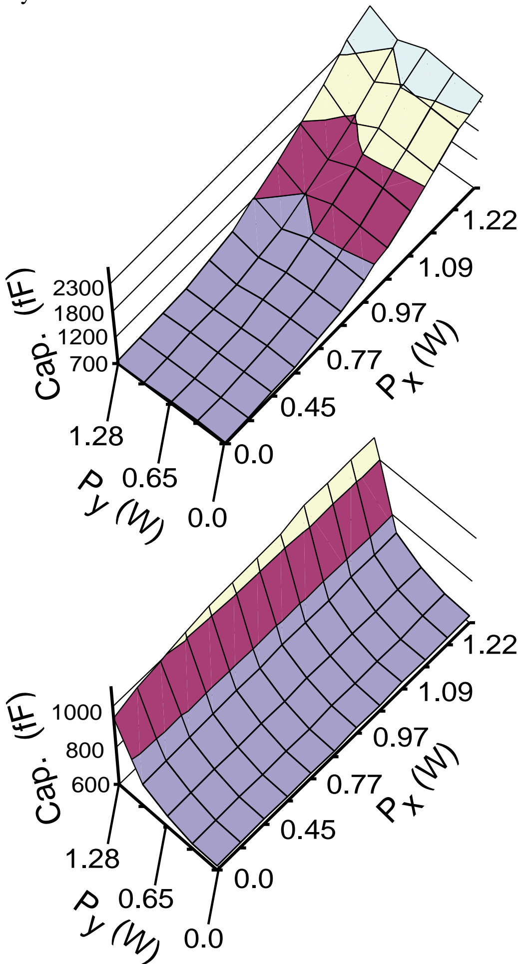

Fig. 9: X-axis capacitance (a-top) and Y-axis capacitance (b-bottom) plotted against input power levels in X and Y actuators.

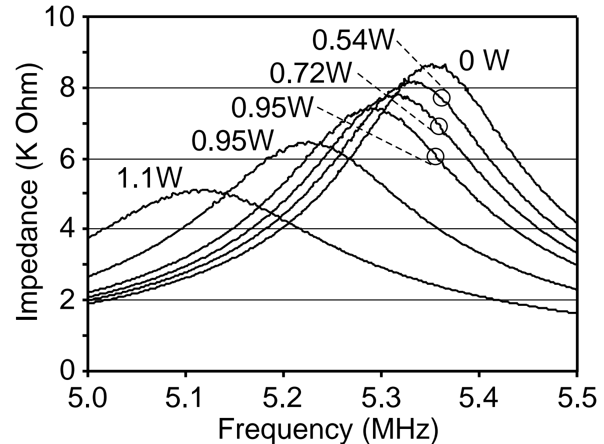

Fig. 10: Applying the resonance method to capacitive position sensing.

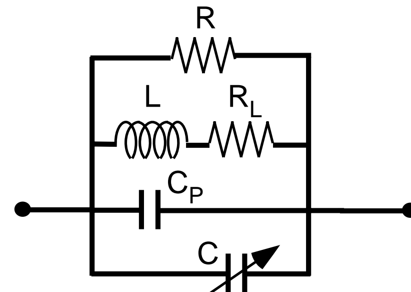

Fig. 11: The electrical equivalent circuit for the resonance measurement.

REFERENCES

[1] T. Hirano, L-S. Fan, W.Y. Lee, J. Hong, T. Semba, W. Imaino, S. Pattanaik, S. Chan, and P. Webb, " A micro-actuator for a hard-disk drive fine tracking servo," ASME Intl. Mech. Eng. Congress & Exposition, New York, pp. 253-260, 1998; also JMEMS 7(2), 6/98.

[2] H. Guckel, K. Fischer, and E. Stiers, "Closed loop controlled, large throw, magnetic linear microactuator with 1000 micron structural height," IEEE, Int. Conf. On Micro Electro Mechanical Systems, pp. 414-418, 1998.

[3] H. Rothuizen, U. Drechsler, G. Genolet, W. Haberle, M. Lutwyche, R. Stutz, R. Widmer, and P. Vettiger, "Fabrication of a micromachined magnetic X/Y/Z scanner for parallel scanning probe applications," Microelectronic Engineering, 53 (2000), pp. 509-512, 2000.

[4] A. Tuantranont, V. M. Bright, J. Zhang, W. Zhang, J. Neff, and Y. C. Lee, "MEMS-controllable microlens array for beam steering and precision alignment in optical interconnect systems," in Solid-State Sensor and Actuator Workshop, Hilton Head, pp. 101-104, 2000.

[5] J.S. Park, L.L. Chu, A. D. Oliver, and Y. B. Gianchandani, "Bent-beam electrothermal actuators-Part II: Linear and rotary microengines," JMEMS, 10(2), pp. 255-262, 2001.

[6] L. Chu, J. A. Hetrick, and Y. B. Gianchandani, "High amplificatin compliant microtransmissions for rectilinear electrothermal actuators," Sensors and Actuators A, 97-98(2002), pp. 776-783, 2002.

[7] Y. B. Gianchandani, and K. Najafi, "Bent-beam strain sensors," IEEE Journal of Microelectromechanical Systems 5(1), pp. 52-58, 1996.

[8] F. Lärmer, A. Schilp," Method of anisotropically etching silicon," US Patent #5501893, German Patent DE4241045.

[9] T.B. Gabrielson, 'Mechanical-thermal noise in micromachined acoustic and vibration sensors," IEEE Trans. on Electron Devices, 40(5), pp. 903-909, 1993.